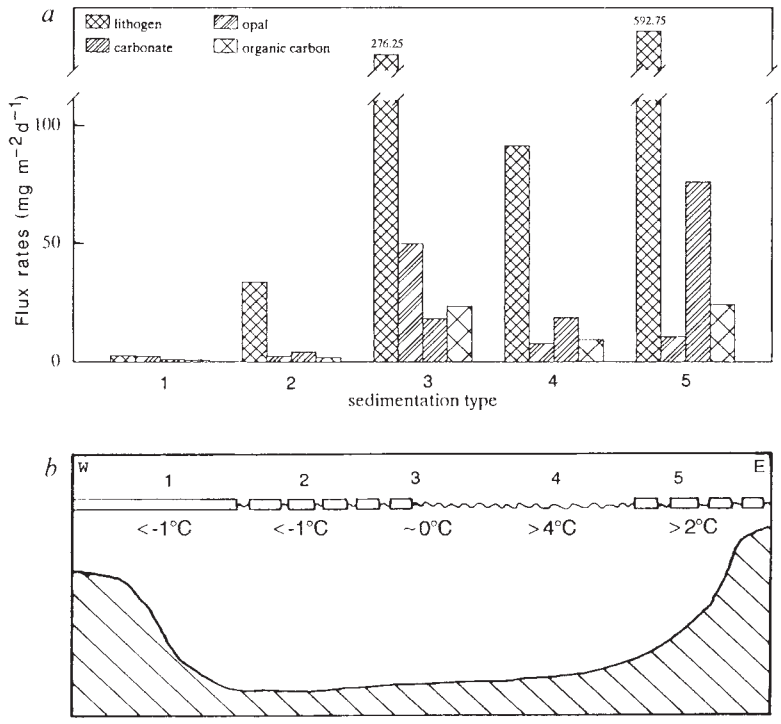

FIG. 3 *a*, Average sedimentation in the five sedimentation regimes of the Fram Strait: (1) closed ice cover above the East Greenland Current; (2) ice cover with open water areas above the East Greenland Current; (3) ice-margin conditions, (4) open water above the West Spitsbergen Current; and (5) ice cover above the West Spitsbergen Current. *b*, Profile through Fram Strait showing different sedimentation situations.

Situations (1) and (2) in the East Greenland Current are characterized by very low fluxes, which seems typical for areas of permanent ice coverage, because similar results were obtained from the ice-covered Weddell Sea[9]. Because no melting can occur in the cold water (<−1 °C) the high portion of lithogenic material in (2) is probably released from the ice by wave wash-off or turning of ice floes[4]. The ice-margin situation (3) is marked by the highest observed opal flux, which can be attributed to favourable conditions for biological productivity. For this as well as for the ice-covered West Spitsbergen Current (situation (4)), the high lithogenic flux results from the release of ice-rafted material by melting. That is also the reason for the high carbonate flux in (5), which is partly composed of ice-transported old carbonates. A high opal flux due to enhanced primary production cannot occur because of the lack of daylight in (5). As indicated by the dominance of fecal pellets in (4) above the West Spitsbergen Current, the high lithogenic flux is caused by high abundances of zooplankton and a high availability of lithogenic material, probably originating from the Barents Sea and transported by the West Spitsbergen Current.

Ice margins will also be found around polynas. Owing to the mode of origin of a polyna, the resulting flux pattern will be similar to that found in (2) in the case of a wind-driven coastal polyna (for example, the East Greenland Shelf polyna[10]) where water temperatures remain cold, or to type (3), if a polyna is caused by the upwelling of water warm enough to melt the ice (for example, the Weddell Sea polyna[11]).

Our sediment-trap data show that high biogenic opal fluxes may be related to summer-ice-margin conditions (Fig. 3). That enhanced opal production that can be recorded may be seen in sediment cores from the Skagerrak/Norwegian Sea and Fram Strait, where diatom maxima were related to past positions of the polar front[12], which during summer roughly follows the ice margin. Opal maxima in sediment cores should therefore allow the average position of the ice margin in summer in the past to be reconstructed. □

Received 18 October; accepted 21 January 1991.

1. Honjo, S. in *Polar Oceanography* (ed. Smith, W.O.) 687–739 (Academic, New York, 1990).
2. Wefer, G. *et al.* in *Geological History of the Polar Oceans: Arctic versus Antarctic* (eds Bleil, U. & Thiede, J.) 363–379 (Kluwer, Dordrecht, 1990).
3. Berner, H. & Wefer, G. in *Geological History of the Polar Oceans: Arctic versus Antarctic* (eds Bleil, U. & Thiede, J.) 317–335 (Kluwer, Dordrecht, 1990).
4. Pfirman, S., Lange, M.A., Wollenburg, I. & Schlosser, P. in *Geological History of the Polar Oceans: Arctic versus Antarctic* (eds Bleil, U. & Thiede, J.) 187–211 (Kluwer, Dordrecht, 1990).
5. Smith, W. O. Jr., Baumann, M. E. M., Wilson, D. L. & Aletsee, L. *J. geophys. Res.* **92,** 6777–6786 (1987).
6. Honjo, S., Manganini, S. J., Karowe, A. & Woodward, B. L. *Tech. Rep. WHOI-87-17* (Woods Hole Oceanographic Institution, Woods Hole, 1987).
7. Honjo, S., Manganini, S. J. & Wefer, G. *Deep-Sea Res.* **35,** 1223–1234 (1988).
8. Wollenburg, I. & Pfirman, S. *Berichte FB Geowissenschaften Univ. Bremen* **6,** 52–57 (1989).
9. Fischer, G. *et al. Nature* **335,** 426–428 (1988).
10. Wadhams, P. in *The Nordic Seas* (ed. Hurdle, B. G.) 21–78 (Springer, New York, 1986).
11. Comiso, J. C. & Gordon, A. L. *J. geophys. Res.* **92,** 2819–2833 (1987).
12. Stabell, B. *Geol. Rundsch* **75,** 175–184 (1986).
13. Vinje, T. E. *Norsk Polarinst. Arbok 1975* 163–174 (1977).

ACKNOWLEDGEMENTS. We thank J. Meincke, J. Carstens and the crew of RV *Polarstern* for their help in deploying and recovering the sediment traps, and M. Botros and W. H. Berger for critical reading of the manuscript and helpful comments. This research was supported by the Bundesminister für Forschung und Technologie (Projekt Framstraße).

Mixing-layer distortion at the confluence of channels of different depth

James L. Best* & André G. Roy†

* Department of Earth Sciences, University of Leeds, Leeds LS2 9JT, UK
† Département de Géographie, Université de Montréal, CP 6128, Montréal, Québec H3C 3J7, Canada

CHANNEL confluences have received considerable recent attention in the fields of geomorphology[1–3], sedimentology[4–9] and hydraulic engineering[10–13]. Where channels join, rapid changes in fluid velocity, turbulence intensity, channel hydraulic geometry and bed geometry may occur[14–17]. Previous models of junction dynamics have tended to assume that the confluent channels are of equal depth[10,18], a condition that may be found only rarely in natural junctions; more often, the depths of confluent channels are different[19]. This discordance is commonly the result of the formation, at the mouth of each confluent channel, of bars that possess steep avalanche faces which dip into a central junction scour[1,2,5,20]. Here we suggest that when channels of different depth join, the mixing layer that forms at their confluence is distorted by

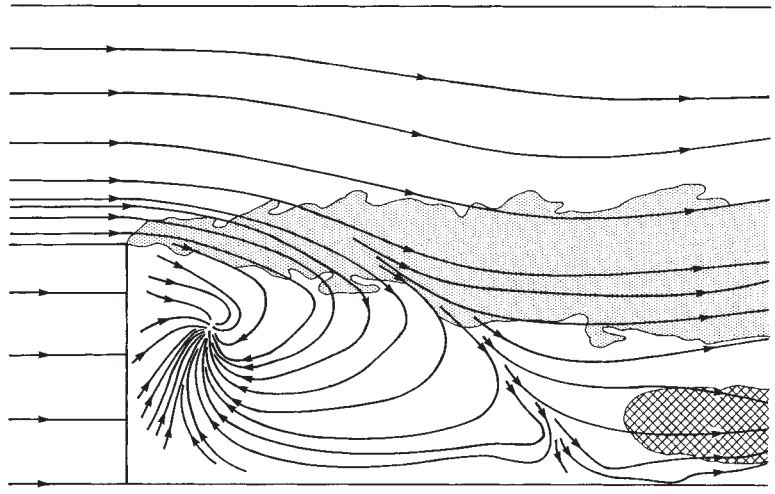

FIG. 1 Bed streamlines and spreading of the mixing layer at a Reynolds number of 12,670. Bed streamlines show the extent of the separation zone behind the step and the entrainment of fluid from the deeper channel. Stippled shading indicates the maximum extent of the mixing layer, and cross-hatching denotes the zone of fluid upwelling produced by deformation of the mixing layer.

interacting with a separation zone which forms in the lee of the mouth of the shallower channel. This mixing-layer distortion imparts a complex three-dimensional flow to the junction, promoting vertical fluid upwelling and significantly enhancing rapid mixing within the flow of the shallow tributary, while retarding the rate of mixing across the flow of the deeper channel. Suspended sediments or contaminants within the deeper channel may be transferred rapidly across the flow of the shallower tributary, upwelling downstream of the junction.

To investigate the dynamics of laterally mixing flows with different depths, we have conducted a series of experiments in a flume consisting of two parallel channels, each 0.135 m wide and 3 m long, which merged at the downstream end of a blunt-ended splitter plate. Flow in one channel was made shallower by inserting a gently tapered ramp, 1.1 m in length, which terminated in a 0.05-m high 90° negative step at the end of the splitter plate (Fig. 2 insert). Flow depths were kept constant, being 0.10 and 0.05 m in the deeper and shallower channels respectively, and were allowed to mix freely downstream from the splitter plate in a channel 0.27 m wide and 3 m long. The results presented here are based on visualization of the mixing flows by injecting dye both at the negative step and on the water surface; bed streamlines were constructed from traces of water-based paint placed on the flume floor. Velocity measurements were made using a DANTEC two-component laser Doppler anemometer. Measurements were made at three mean Reynolds numbers, and in each experiment there was a slight difference in velocity between the two confluent flows, the shallower channel being between 0.83 and 0.99 times the velocity in the deeper channel.

The mixing of two flows of different depths essentially involves interaction between the mixing layer that forms where the flows meet and a zone of separated flow formed in the lee of the step. Bed streamlines and the time-averaged position of the mixing layer at a mean Reynolds number of 12,670 (Fig. 1) illustrate that the separation zone possesses a complex three-dimensional recirculation as a result of interaction with the mixing layer. A nodal point of upwelling fluid is present within the separation zone approximately one step height downstream of the step edge. The length of the separation zone, defined by its maximum downstream extent along the wall of the flume, remained constant at 3.5 step heights for all three Reynolds numbers studied. Deformation of the mixing layer closely follows the curvature of bed streamlines around the separation zone (Fig. 1). At each Reynolds number, the rate of mixing-layer growth decreases at a certain distance downstream (Fig. 2). The distance to this point of change in rate decreases at higher Reynolds number, reflecting the increasing entrainment of fluid into the separation zone from the mixing layer and deeper channel. Another possible consequence of increased fluid entrainment into the separation zone is that, at a given position downstream, the mixing layer becomes narrower at higher Reynolds numbers (Fig. 2). Therefore, as the Reynolds number increases, suspended sediments or contaminants will increasingly tend to become entrained into the separation zone, enhancing mixing across the flow of the shallower channel but retarding mixing across the flow of the deeper channel downstream of the confluence.

Fluid within the mixing layer is also considerably distorted in three dimensions through interaction with the separation zone. The mixing layer is characterized by Kelvin-Helmholtz instabilities which may pair, split and coalesce as they convect downstream[21]. In the presence of the separation zone, these vortices are gradually distorted as they travel downstream, their bases being deformed inwards towards the separation zone as revealed by the bed streamlines (Fig. 1). Vortices that originate with vertical axes in the initiation zone of the mixing layer are gradually deformed and adopt a vorticity that has its axis in the cross-stream plane (Fig. 3). The vortex bases are drawn progressively towards the wall of the shallower channel and, as vortex stretching and break-up occurs, fluid from the mixing layer (and the deeper channel) upwells within the body of the shallower-channel flow downstream from the separation zone (Figs 1 and

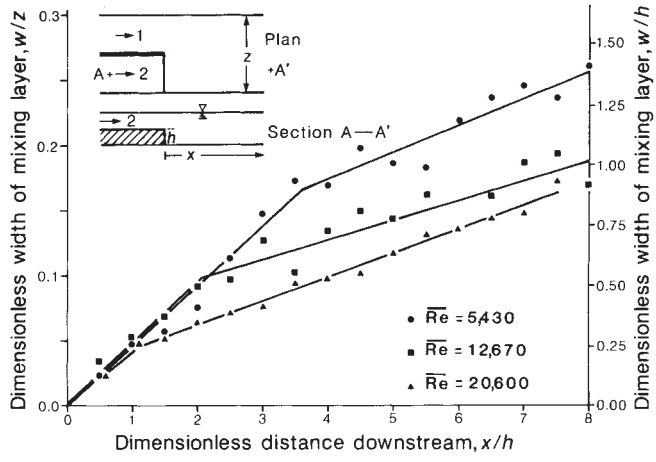

FIG. 2 Spreading rate of the mixing layer for the three mean Reynolds numbers examined. The width of the mixing layer is made dimensionless by dividing either by the channel width z or by the step height h. The downstream distance, x, has its origin at the step edge and is made dimensionless by dividing by the step height.

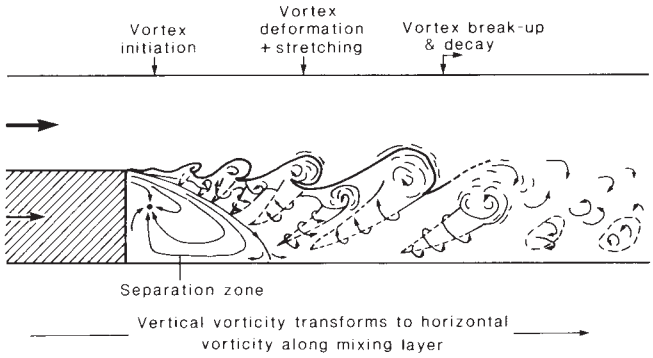

FIG. 3 A schematic model of mixing-layer distortion at the confluence of two flows of different depth. This planform diagram illustrates that deformation of the vertical mixing-layer vortices leads to the production of horizontal vorticity, enhanced mixing and fluid upwelling downstream of the confluence.

3). In Fig. 3 we illustrate a schematic model of this process of vortex and mixing-layer distortion.

Such complex three-dimensional deformation of the mixing layer is characteristic of all the unequal-depth mixing flows that we have studied. Although we have examined only zero degree confluence angles, mixing-layer distortion such as that described here can be expected at any junction in which the confluent channels are of different depths. The orientation of the separation zone is controlled by the planform geometry of the negative step, which in natural channels is formed by avalanche faces of tributary mouth bars which dip into the central confluence scour[1,5,6]. Consequently, the degree of entrainment of deeper-channel fluid into the separation zone and the position of the zone of upwelling will be dependent on the position of the tributary mouth bars, this itself being controlled by the junction angle and the ratio of discharges between the confluent channels[2,5,18]. This process of mixing-layer distortion and fluid upwelling may be invoked to explain patterns of fluid mixing at natural river junctions[22,23] where fluid from one channel is observed to upwell within the body of the other tributary flow downstream from the confluence.

The process we have outlined here has many implications. The dispersal of sediment at junctions across channel towards the shallower tributary may be greatly enhanced by such a depth differential between the confluent channels. This may influence erosion, through the position of the mixing layer and its associated higher Reynolds stresses, and deposition through control of the location of both zones of upwelling and the principal sediment transport pathways. Helical flow cells, which have been described at river channel confluences[1,20], may also originate from such depth-differential-controlled processes and not from any inherent helical flow where flows of equal depth combine. Attempts at modelling the near-field of side discharges in effluent dispersal[24] must also account for this mixing-layer distortion, which may significantly increase the potential for mixing across the shallower channel at a junction while simultaneously decreasing the rate of mixing across the deeper channel. Thus, effluents suspended in a deep channel may be rapidly transferred across the flow of a shallower channel when the two flows merge. □

Received 19 November 1990; accepted 18 February 1991.

1. Mosley, M. P. *J. Geol.* **84,** 535–562 (1976).
2. Ashmore, P. E. & Parker, G. *Water Resour. Res.* **19,** 342–402 (1983).
3. Roy, A. G. & Bergeron, N. *Geomorphology* **3,** 99–112 (1990).
4. Klassen, G. J. & Vermeer, K. *Proc. Int. Conf. Fluvial Hydraul.* Budapest, 1–14 (1988).
5. Best, J. L. *Sedimentology* **35,** 481–498 (1988).
6. Mosley, M. P. & Schumm, S. A. *Econ. Geol.* **72,** 691–694 (1977).
7. Reid, I., Best, J. L. & Frostick, L. E. in *Floods: Hydrological, Sedimentological and Geomorphological Implications* (eds Beven, K. & Carling, P.) 135–150 (Wiley, Chichester, 1989).
8. Bryant, I. D., Holyoak, D. T. & Mosely, K. A. *Proc. Geol. Ass.* **94(4),** 321–343 (1983).
9. Best, J. L. & Brayshaw, A. C. *J. geol. Soc. Lond.* **142,** 747–755 (1985).
10. Soong, H. K. thesis, Univ. Connecticut (1976).
11. Hager, W. H. *J. hydraul. Engng* **115,** 243–259 (1989).
12. Sutherland, A. J. in *Proc. 9th Aus. Fluid Mech. Conf.* 259–263 (Univ. of Auckland, 1986).
13. Chu, V. H. & Babarutsi, S. *J. hydraul. Engng* **114,** 1257–1274 (1988).
14. Richards, K. S. *Water Resour. Res.* **16,** 241–244 (1980).
15. Best, J. L. & Reid, I. *J. hydraul. Engng* **110,** 1588–1594 (1984).
16. Roy, A. G. & Woldenberg, M. J. *J. Geol.* **94,** 401–411 (1986).
17. Roy, A. G. & Roy, R. *Earth Surf. Proc. Landf.* **13,** 77–84 (1988).
18. Best, J. L. *Soc. Econ. Palaeontalogists and Mineralogists spec. Publ.* **39,** 27–35 (1987).
19. Kennedy, B. A. *Earth Surf. Proc. Landf.* **9,** 153–173 (1984).
20. Ashmore, P. E. *Earth Surf. Proc. Landf.* **7,** 201–225 (1982).
21. Winant, C. D. & Browand, F. K. *J. Fluid Mech.* **63,** 237–255 (1974).
22. Sternberg, H. O. *The Amazon River of Brazil* 74 (Steiner, Weisbader, 1975).
23. Roy, A. G. & De Serres, B. *Bull. Soc. Géog. Liège* **25,** 113–127 (1989).
24. McGuirk, J. J. & Rodi, W. *J. Fluid Mech.* **86,** 761–781 (1978).

ACKNOWLEDGEMENTS. We thank the Earth Sciences workshop at Leeds for construction of the mixing-flow apparatus. Travel for A.G.R. was made possible through a grant from FCAR; this paper was prepared while J.L.B. held a Royal Society/NSERC Anglo-Canadian Scientific Exchange Scheme Fellowship at the Université de Montréal that was also supported by the Foundation for Canadian Studies. We are grateful for the thoughtful comments of Jim Pizzuto.

Microbial reduction of uranium

Derek R. Lovley, Elizabeth J. P. Phillips, Yuri A. Gorby & Edward R. Landa

Water Resources Division, 430 National Center, US Geological Survey, Reston, Virginia 22092, USA

REDUCTION of the soluble, oxidized form of uranium, U(VI), to insoluble U(IV) is an important mechanism for the immobilization of uranium in aquatic sediments and for the formation of some uranium ores[1–10]. U(VI) reduction has generally been regarded as an abiological reaction in which sulphide, molecular hydrogen or organic compounds function as the reductant[1,2,5,11]. Microbial involvement in U(VI) reduction has been considered to be limited to indirect effects, such as microbial metabolism providing the reduced compounds for abiological U(VI) reduction and microbial cell walls providing a surface to stimulate abiological U(VI) reduction[1,12,13]. We report here, however, that dissimilatory Fe(III)-reducing microorganisms can obtain energy for growth by electron transport to U(VI). This novel form of microbial metabolism can be much faster than commonly cited abiological mechanisms for U(VI) reduction. Not only do these findings expand the known potential terminal electron acceptors for microbial energy transduction, they offer a likely explanation for the deposition of uranium in aquatic sediments and aquifers, and suggest a method for biological remediation of environments contaminated with uranium.

It is becoming increasingly clear that the reduction of metals in anaerobic environments is often the result of the direct enzymatic reduction by bacteria[14,15]. For example, the Fe(III)-reducing microorganism, strain GS-15, grows under anaerobic conditions by enzymatically coupling the oxidation of acetate to carbon dioxide with the reduction of Fe(III) to Fe(II)[16,17] according to:

$$CH_3COO^- + 8Fe(III) + 4H_2O \rightarrow 8Fe(II) + 2HCO_3^- + 9H^+$$

Thermodynamic calculations have indicated that, per electron transferred, acetate oxidation coupled to U(VI) reduction has the potential to yield more than twice the energy that is available from Fe(III) reduction[8]. When GS-15, grown on acetate and Fe(III), was inoculated into an anaerobic medium with acetate as the sole electron donor and U(VI) as the potential electron acceptor, U(VI) was reduced to U(IV) over time (Fig. 1*a*). Growth coincided with U(VI) reduction and stopped as U(VI) became depleted. When [2-^{14}C]-acetate was incorporated into the medium, $^{14}CO_2$ was generated in direct proportion to U(VI) reduction (Fig. 1*b*). In a separate experiment in which acetate concentrations were measured in cultures growing with U(VI) reduction, U(VI) and acetate loss over time were linearly related (correlation coefficient $r = 0.9$) with a U(VI)/acetate ratio of